Manuscript chem.202005289.R1 for *Chemistry – A European Journal* (Article)

Reactions of Late First-Row Transition Metal (Fe–Zn) Dichlorides with a PGeP Pincer Germylene

Ana Arauzo,[a] Javier A. Cabeza,*[b] Israel Fernández,[c] Pablo García-Álvarez,[b] Inés García-Rubio,[a,d] and Carlos J. Laglera-Gándara[b]

[a] *Instituto de Nanociencia y Nanomateriales de Aragón (INMA), CSIC-Universidad de Zaragoza, 50009 Zaragoza, Spain.*

[b] *Centro de Innovación en Química Avanzada (ORFEO-CINQA), Departamento de Química Orgánica e Inorgánica, Universidad de Oviedo, 33071 Oviedo, Spain. E-mail: jac@uniovi.es*

[c] *Centro de Innovación en Química Avanzada (ORFEO-CINQA), Departamento de Química Orgánica I, Facultad de Ciencias Químicas, Universidad Complutense de Madrid, 28040 Madrid, Spain.*

[d] *Centro Universitario de la Defensa, Academia General Militar, 50090 Zaragoza, Spain.*

Supporting Information and the ORCID identification numbers for the authors of this article can be found under: https://doi.org/10.1002/chem.20yyxxxxx.

Abstract

The reactivity of the PGeP germylene 2,2'-bis(di-*iso*propylphosphanylmethyl)-5,5'-dimethyldipyrromethane-1,1'-diylgermanium(II), Ge(pyrmP^{i}Pr$_2$)$_2$CMe$_2$, with late first raw transition metal (Fe–Zn) dichlorides has been investigated. All reactions led to PGeP pincer chloridogermyl complexes. The reactions with $FeCl_2$ and $CoCl_2$ afforded paramagnetic square planar complexes of formula [MCl{κ^3*P*,*Ge*,*P*-GeCl(pyrmP^{i}Pr$_2$)$_2$CMe$_2$}] (M = Fe, Co). While the iron complex maintains an intermediate spin state (S^1; μ_{eff} = 3.0 μ_B) over the temperature range 50–380 K, the effective magnetic moment of the cobalt complex varies linearly with temperature from 1.9 μ_B at 10 K to 3.6 μ_B at 380 K, indicating a spin crossover behavior that involves $S^{1/2}$ (predominant at T < 180 K) and $S^{3/2}$ (predominant at T > 200 K) species. Both cobalt(II) species have been detected by EPR at T < 20 K. The reaction of Ge(pyrmP^{i}Pr$_2$)$_2$CMe$_2$ with [NiCl$_2$(dme)] (dme = dimethoxyethane) gave a square planar nickel(II) complex, [NiCl{κ^3*P*,*Ge*,*P*-GeCl(pyrmP^{i}Pr$_2$)$_2$CMe$_2$}], whereas the reaction with $CuCl_2$ involved a redox process that rendered a mixture of the germanium(IV) compound GeCl$_2$(pyrmP^{i}Pr$_2$)$_2$CMe$_2$ and a binuclear copper(I) complex, [Cu$_2${μ-κ^3*P*,*Ge*,*P*-GeCl(pyrmP^{i}Pr$_2$)$_2$CMe$_2$}$_2$], whose metal atoms are in tetrahedral environments. The reaction of the germylene with $ZnCl_2$ led to the tetrahedral derivative [ZnCl{κ^3*P*,*Ge*,*P*-GeCl(pyrmP^{i}Pr$_2$)$_2$CMe$_2$}].

Introduction

The use of pincer ligands in transition metal (TM) complexes is currently a hot research topic because the balance between reactivity and stability often provided by these ligands to their metal complexes is a key factor for the excellent catalytic applications that have been found for many of these complexes.[1,2] As strong electron-donating ligands are frequently required to prepare catalytically efficient metal complexes, many pincer ligands having an N-heterocyclic carbene (NHC) as the central *C*-donor group have already been reported.[3] However, although the heavier carbene analogues (silylenes, germylenes and stannylenes) are also very strong electron-donating groups[4] and some of their metal complexes have already demonstrated an excellent ligand behavior in catalytic reactions,[5,6] their participation in pincer complexes is still limited to a few ECE,[6j-l,7] ENE,[6d,6h,6i,6n] and PEP [8–14] systems (E = Si, Ge or Sn).

Regarding metal-free PGeP pincer-type germylenes,[15] only six members of this family are currently known. We reported the first one in 2017 (compound **A** in Figure 1)[10] and we managed to prepare some d^8 metal (Rh, Ir, Ni, Pd, Pt) complexes with it,[16] but the short length of its CH$_2$P^{t}Bu$_2$ sidearms resulted in very distorted square geometries and we failed to isolate any d^{10} metal derivative. Subsequently, Goicoechea's group reported the second PGeP germylene (compound **B** in Figure 1),[11] but it did not behave as a pincer ligand in its metal derivatives because its small 5-membered

$GeNC_2N$ ring forces a long separation between the P atoms, impeding their binding to the same metal atom. Looking for a more flexible ligand framework, we set out the synthesis of germylene **C** (Figure 1), but the little steric protection of its Ge atom resulted in low stability of the TM derivatives that were prepared.[12] To improve this situation we have recently synthesized germylene **E** (Figure 1),[13] which is based on the dipyrromethane scaffold, and we have already proven that it forms stable d^{10} metal derivatives.[13,17] Although two additional metal-free PGeP germylenes have been recently communicated (**D** and **F** in Figure 1), germylene **D** has only been used as a ligand in nickel(0) complexes[14] and no reaction with a TM complex has yet been reported for germylene **F**.[18]

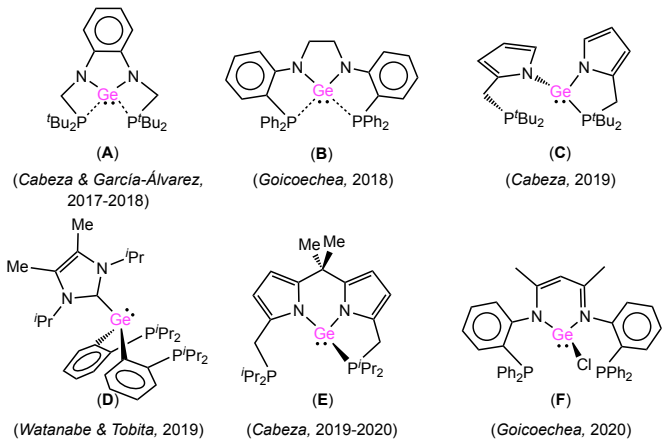

Figure 1. The currently known metal-free PGeP germylenes.

We now report the reactivity of germylene **E** with the lightest metal dichlorides of groups 8–12 of the Periodic Table (Fe–Zn). These reactions have afforded stable chloridogermyl PGeP pincer complexes of earth-abundant metals whose metal atoms are in unstrained square planar (Fe^{II}, Co^{II}, Ni^{II}) or tetrahedral (Cu^{I}, Zn^{II}) ligand environments. Also, very interesting magnetic properties have been observed for the paramagnetic (Fe, Co) complexes: while the iron(II) complex maintains an intermediate spin state (S^1) in the temperature range 50–380 K, the cobalt(II) complex presents an unusual temperature-dependent spin crossover equilibrium between low ($S^{1/2}$) and high spin ($S^{3/2}$) species that extends between 10 and 380 K. It is also noteworthy that the reaction of germylene **E** with $CuCl_2$ proceeds through an unexpected redox process that leads to a binuclear copper(I) complex containing an almost planar inorganic six-membered $Cl_2Cu_2Ge_2$ ring.

Results and discussion

Iron(II) and cobalt(II) complexes

Pale brown and yellow-orange solids were isolated in good yields from the reactions of germylene **E** with $FeCl_2$ and $CoCl_2$, respectively (Scheme 1). Their microanalytical and mass spectral data, in

addition to the previously known tendency of germylenes to get their Ge atom inserted into M–Cl bonds,[11-13,17] were consistent with the formula [MCl{κ^3*P*,*Ge*,*P*-GeCl(pyrmP^{i}Pr$_2$)$_2$CMe$_2$}], M = Fe (**1**), Co (**2**). Compounds **1** and **2** are the first PGeP pincer iron and cobalt complexes to be reported.

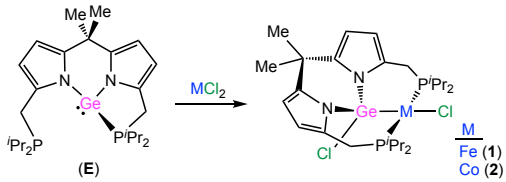

Scheme 1. Synthesis of complexes **1** and **2**.

No single crystals of compound **1** could be obtained, but an X-ray diffraction (XRD) study on a crystal of compound **2** (data taken at 157 K) revealed that it was constituted by square planar cobalt(II) molecules in which the metal atom is attached to a chloridogermyl PGeP pincer ligand (Figure 2) with a Co–Ge distance of 2.2519(5) Å. This molecule reminds that of the only previously known square planar complex derived from germylene **E**, that is [PdCl{κ^3*P*,*Ge*,*P*-GeCl(pyrmP^{i}Pr$_2$)$_2$CMe$_2$}], which was prepared by treating the T-shaped palladium(0) complex [Pd{κ^3*P*,*Ge*,*P*-Ge(pyrmP^{i}Pr$_2$)$_2$CMe$_2$}] with HCl or, alternatively, by reacting germylene **E** with [PdCl$_2$(MeCN)$_2$].[18]

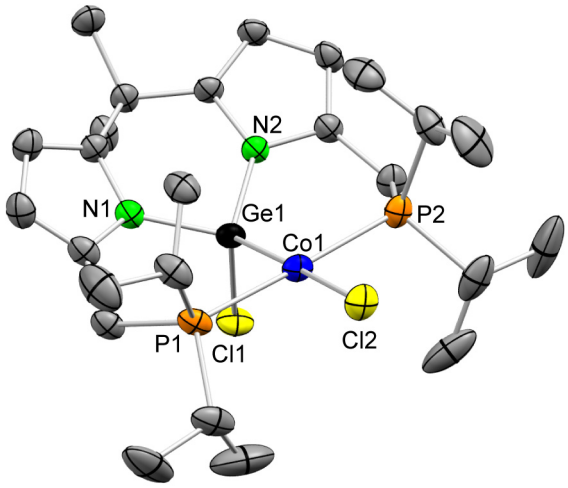

Figure 2. XRD molecular structure of complex **2** (157 K, 30% displacement ellipsoids, H atoms have been omitted for clarity). Selected bond lengths (Å) and angles (°): Co1−P1 2.245(1), Co1−P2 2.253(1), Co1−Ge1 2.2519(5), Co1−Cl2 2.2353(8), Ge1−Cl1 2.2200(9), Cl1−Ge1−Co1 112.55(3), Ge1−Co1−Cl2 178.46(4), P1−Co1−P2 178.02(4).

Variable temperature magnetic susceptibility studies were performed on complexes **1** and **2** (Supporting Information, Figure S17), not only to investigate their magnetic behavior but also to get more insights into their molecular structures (both compounds could be tetrahedral or square planar). Figure 3 shows that the effective magnetic moment (μ_{eff}) of the iron(II) complex **1** is *ca.* 3.0 μ_B over a wide temperature range (50–380 K), being smaller at T < 50 K probably due to thermal depopulation of zero-field split electronic states.[19] Aiming at interpreting the magnetic behavior of complex **1** and

taking into account the various spin states that are possible for a d^6 metal in tetrahedral and square planar ligand environments (Figure 4), the relative stabilities in the gas phase of the possible structure/spin state combinations for compound **1** were computed by DFT methods using three different calculation levels. Table 1 shows that the tetrahedral (TD) structure is systematically the most stable one regardless the functional used, but the square planar (SQ) with intermediate spin (IS) state (S^1) is only a little less stable. Given that the experimental magnetic moment of compound **1** is 3.0 μ_B, we propose that, in the solid state, compound **1** is an IS SQ species. In addition, the observed variation of the effective magnetic moment with the temperature could be nicely modelled in terms of an isolated S^1 system described by the spin hamiltonian, $\mathcal{H} = D\left[S_z^2 - \frac{1}{3}S(S+1)\right] - \mu_B \vec{H}\hat{g}\vec{S}$, with an isotropic g = 2.10(5) and an axial zero field splitting term D/k_B = 20(5) K. These results correspond well to previously reported parameters for SQ IS iron(II) complexes.[20] While most four-coordinate iron(II) complexes are TD S^2 species, SQ S^1 complexes are not scarce,[20-22] being well represented by porphyrin derivatives.[22] On the other hand, high spin (HS) SQ iron(II) complexes (S^2) are very rare and require hard π-donor ligands.[23]

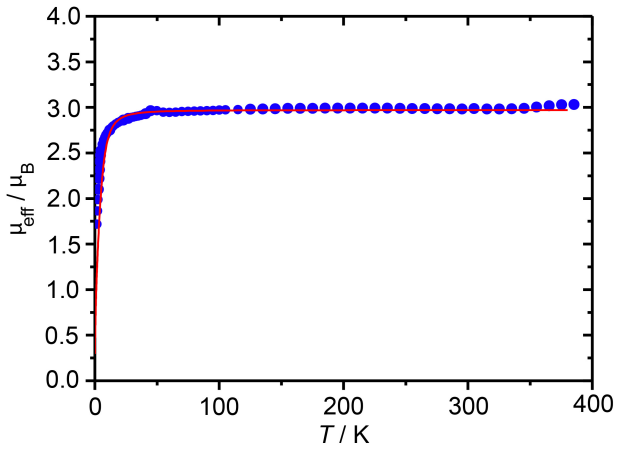

Figure 3. Temperature dependence of the effective magnetic moment of compound **1** (solid sample). Data (blue circles) have been fitted (red line) with g = 2.10(5) and D/k_B = 20(5) K.

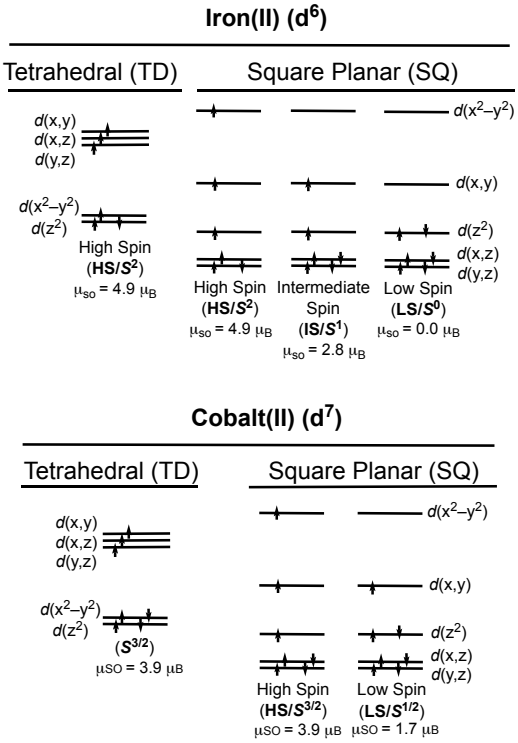

Figure 4. Possible spin states for iron(II) and cobalt(II) in tetrahedral and square-planar ligand environments.

Table 1. DFT-calculated relative energies (kcal mol^{-1}) for the possible structure/spin state combinations of complex **1**[a]

DFT level	TD/HS (S^2)	SQ/HS (S^2)	SQ/IS, (S^1)	SQ/LS, (S^0)
B3LYP-D3/def2SVP	0.0	7.6	2.0	31.1
CAM-B3LYP-D3/def2SVP	0.0	8.0	1.7	2.3
PBE0-D3/def2SVP	0.0	7.2	3.2	36.9

[a]TD = tetrahedral, SQ = square-planar, HS = high spin, IS = intermediate spin, LS = low spin.

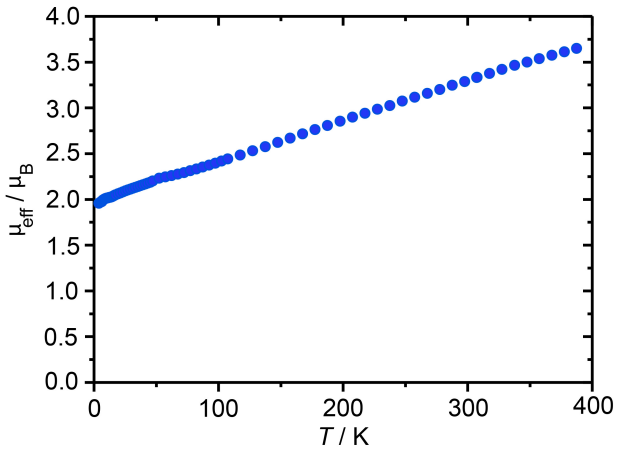

Figure 5. Temperature dependence of the effective magnetic moment of compound **2** (solid sample).

The thermal behavior of the magnetic moment of the cobalt(II) complex **2** is remarkably unusual, as a continuous increase of the temperature resulted in a continuous increase of μ_{eff}, which varies from 1.9 μ_B at 10 K to 3.6 μ_B at 380 K (Figure 5). Such a behavior implies the existence of an

equilibrium in the solid state involving two species of different spin states, S = 1/2 (μ_{so} = 1.7 μ_B) and S = 3/2 (μ_{so} = 3.9 μ_B). Spin crossovers are frequently observed in paramagnetic complexes but they generally occur in the proximity of a given temperature (abrupt spin change).[24] Gradual spin crossovers that extend over several hundred degrees are unusual.[25]

Table 2. DFT-calculated relative energies (kcal mol^{-1}) for the possible structure/spin state combinations of complex **2**[a]

DFT level	TD ($S^{3/2}$)	SQ/HS ($S^{3/2}$)	SQ/LS, ($S^{1/2}$)
B3LYP-D3/def2SVP	0.0	9.0	1.1
CAM-B3LYP-D3/def2SVP	4.9	7.7	0.0
PBE0-D3/def2SVP	8.8	16.4	0.0

[a]TD = tetrahedral, SQ = square-planar, HS = high spin, LS = low spin.

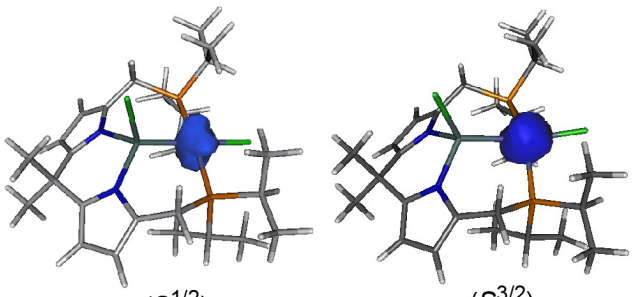

Figure 6. Spin density plots for the square planar $S^{1/2}$ and $S^{3/2}$ species of complex **2**.

Given the possible combinations of structures and spin states for four-coordinate d^7 complexes (Figure 4), the magnetic measurements (Figure 5) and the low temperature (157 K) XRD structure of complex **2** (Figure 2) made it clear that the $S^{1/2}$ species has a SQ structure. Regarding the structure of the $S^{3/2}$ species, although DFT calculations (Table 2) indicated that, in the gas phase, the TD structure is more stable than the SQ one, the difficulty of a TD to SQ isomerization in the solid state suggested that the $S^{3/2}$ species is also SQ. Such a proposal was confirmed by an XRD structure determination at 298 K (Supporting Information, Figure S14, Table S1), which shows a molecular structure very similar to that depicted in Figure 2 (the most notable difference resides in the Co–P bond lengths, which are a bit longer in the 298 K structure (2.2500(9) and 2.2562(9) Å) than in the 157 K structure (2.245(1) and 2.253(1) Å), but with notably different unit cell parameters: a = 11.4752(2) Å (157 K), 11.5537(4) Å (298 K); b = 18.4482(4) Å (157 K), 18.6335(6) Å (298 K); c = 14.5885(3) Å (157 K), 14.6533(5) Å (298 K); v = 2749.6(2) Å^3 (157 K), 3014.1(2) Å^3 (298 K). As the spin densities of the SQ $S^{1/2}$ and $S^{3/2}$ species are located on the metal atoms (Figure 6), only metal-based orbitals should be involved in the spin crossover; therefore, the metal–ligand bond lengths and angles of the $S^{1/2}$ and $S^{3/2}$ species should not be very different. However, very small variations of the metal–ligand bond lengths should notably modify the distances between non-bonded atoms of the edge of the molecule, affecting the molecule packing and the unit cell parameters.[26] As spin crossovers are driven by molecular changes, a very small strecht of some metal–ligand bond distances

provokes in this case a (subtle) weakening of the ligand field that favors the $S^{3/2}$ spin state at increasing temperatures. For cobalt(II), both TD and LS SQ complexes are well represented in the literature,[27] but HS SQ complexes are rare.[23b,28]

We also measured the magnetic moments of compounds **1** and **2** in dichloromethane solution at 25 °C (by NMR, Evans method[29]). That of the iron complex, μ_{eff} = 4.1 μ_B, is higher than that measured in the solid state, μ_{eff} = 3.0 μ_B, probably due to the presence of a small amount of HS TD species (S^2) in solution at that temperature. The solution magnetic moment measured for the cobalt complex, μ_{eff} = 3.1 μ_B, matches that obtained in the solid state at 25°, indicating that the ratio of $S^{1/2}$ to $S^{3/2}$ species does not change from the solid state to the solution.

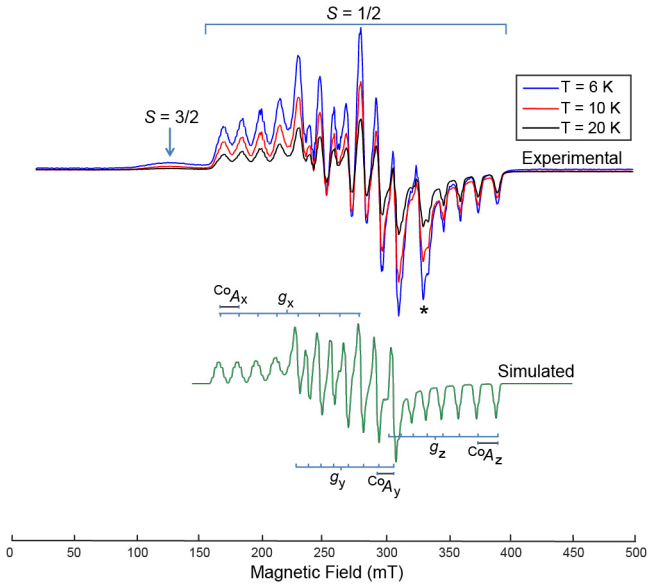

Figure 7. Experimental X-Band CW-EPR spectra of compound **2** in frozen toluene solution (top; microwave power 0.20 mW (6 K) and 0.77 mW (10 and 20 K), field modulation amplitude 0.5 mT; the asterisk indicates a spurious line due to a small amount of an uncharacterized impurity) and simulated spectrum of the $S^{1/2}$ species (bottom; g_x = 3.00, g_y = 2.48, g_z = 1.94; $^{Co}A_x$ = 650 MHz, $^{Co}A_y$ = 375 MHz, $^{Co}A_z$ = 330 MHz, $^{P}A_x$ = 100 MHz, $^{P}A_y$ = 50 MHz, $^{P}A_z$ = 50 MHz, $^{Cl}A_x$ = 80 MHz).

The non-integer values of the spin states of the $S^{3/2}$ and $S^{1/2}$ species of the cobalt(II) compound **2** prompted us to perform an EPR study (Figure 7). The low temperature spectra in frozen toluene solution display three groups of eight lines reflecting the hyperfine interaction of the electron spin with the ^{59}Co nucleus (I = 7/2) and an anisotropic g-tensor. Additionally, a broad line at *ca.* 125 mT (g = 5.4) with no resolved ^{59}Co hyperfine structure could be clearly observed at 6 K, but its relative intensity rapidly decreased, with respect to that of the other signals, as the temperature increased, being barely detected above 20 K. This signal could not be saturated with the highest power available. This behavior is a consequence of short spin relaxation times, typical for cobalt(II) $S^{3/2}$ species. On the other hand, the remaining signals could be observed up to 150 K and saturated with microwave power, indicating their LS ($S^{1/2}$) character. Relative quantification of these two species could not be precisely established because the remaining features associated with the $S^{3/2}$ species could not be observed,

probably because they are very broad and buried under the spectrum of the $S^{1/2}$ species. However, an approximate $S^{3/2}/S^{1/2}$ ratio of 1/10 can be estimated based on the intensities found at 6 K and under the assumption that the *g*-anisotropy is in the range found for other $S^{3/2}$ cobalt(II) centers.[30] It is worth noting that the loss of the low-field signal ($S^{3/2}$ species) with temperature does not necessarily mean that there are no $S^{3/2}$ species at higher temperatures; on the contrary, it is consistent with the behavior of an $S^{3/2}$ spin system, whose signal broadens beyond detection due to typically fast relaxation times upon increasing temperature.

The main features of the $S^{1/2}$ species EPR spectrum could be successfully simulated (Figure 7, green line) using the *g* and ^{59}Co-hyperfine values given in the figure caption. In addition, and especially evident in the high-field features, every line displays a somewhat resolved 1:2:1 triplet due to the hyperfine interaction of the unpaired electron with the nuclei of the two equivalent ^{31}P atoms (I = 1/2, 100%) that are attached to the Co atom. This was simulated in the figure with a superhyperfine coupling. On the other hand, the low-field lines show an appreciably larger linewidth and an additional superimposed hyperfine structure that is not completely resolved and that may be due to coupling to the metal-bound chlorido ligand (^{35}Cl, I = 3/2, 76%; ^{37}Cl, I = 3/2, 24%). The *g*- and ^{Co}A-values are assumed to be collinear and the low-field *g*-value has been associated to a direction in the plane of the ligands. Note that the hyperfine splittings caused by the nuclei of the ligands, ^{P}A and $^{Cl}A_{x,}$ are quite large, similar to what has been found in a cobalt(II) complex that had resolved hyperfine interaction with four equivalent in-plane ^{31}P nuclei[31] and of the same order of magnitude as that found for cobalt(II) porphyrin and phthalocyanine complexes.[32] Large hyperfine splittings have been associated to an occupation of the d(z^2) orbital by the unpaired electron, wherein there is some spin density directed towards the ligands.[32]

Nickel(II) copper(I) and zinc(II) complexes

The reaction of [$NiCl_2$(dme)] (dme = 1,2-dimethoxyethane) with germylene **E** proceeded quickly in toluene at room temperature, affording the mononuclear diamagnetic complex [NiCl{κ^3*P*,*Ge*,*P*-GeCl(pyrmP^{t}Bu$_2$)$_2$}] (**3**) (Scheme 2).

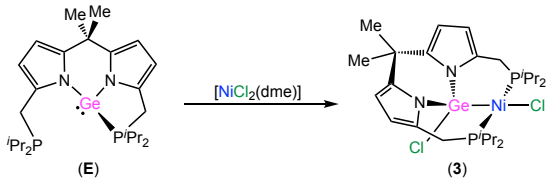

Scheme 2. Synthesis of complex **3**.

The symmetric structure suggested by NMR (^{1}H, ^{13}C{^{1}H} and ^{31}P{^{1}H}) for complex **3**, which located the CMe_2 group methyls in the symmetry plane and showed diastereotopic protons for the CH_2 and P^{i}Pr$_2$ groups, was confirmed by XRD (Figure 8). The structure is very similar to that of

complex **2**, with the Ni atom in a square planar coordination, having the Ge–Ni distance, 2.2173(3) Å, slightly shorter than the Ge–Co distance of complex **2**, 2.2519(5) Å. Analogous PGeP chloridogermyl nickel(II) complexes have been previously prepared from germylenes **A**[16b] and **C**[12] (Figure 1); however, they proved to be more unstable toward oxygen and moisture than complex **3** because the germyl ligand derived from germylene **A**, equipped with short $CH_2P^tBu_2$ sidearms, tends to separate the P atoms from the metal atom and the Ge atom of the germyl ligand derived from germylene **C** has a small steric protection.

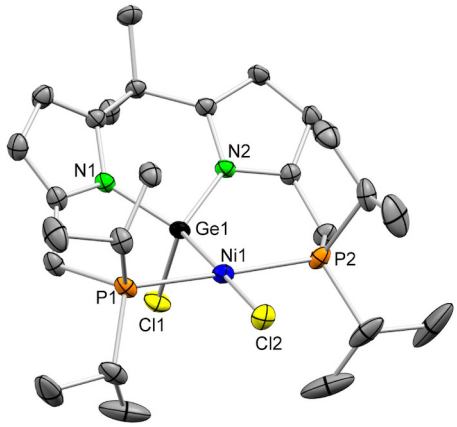

Figure 8. XRD molecular structure of complex **3** (30% displacement ellipsoids, H atoms have been omitted for clarity). Selected bond lengths (Å) and angles (°): Ni1−P1 2.2142(6), Ni1−P2 2.2189(6), Ni1−Ge1 2.2173(3), Ge1−Cl1 2.2180(5), Ni1−Cl2 2.1974(5); Cl1−Ge1−Ni1 112.48(2), Ge1−Ni1−Cl2 178.31(2), P1−Ni1−P2 178.33(2).

The reaction of germylene **E** with $CuCl_2$ in a 1/1 mol ratio in THF at room temperature gave a mixture of several reaction products, including paramagnetic species, which could not be separated and identified. Testing other stoichiometries, we found that the use of a 3/2 **E** to $CuCl_2$ mole ratio afforded a mixture of two diamagnetic products that were easily separated by their different solubility and that were subsequently identified as $[Cu_2\{\mu\text{-}\kappa^3P,Ge,P\text{-}GeCl(pyrmP^tBu_2)_2CMe_2\}_2]$ (**4**) and $GeCl_2(pyrmP^tBu_2)_2CMe_2$ (**5**) (Scheme 3). Complex **4** was fully characterized (including XRD) and compound **5** was identified by comparing its NMR data with those of an authentic sample prepared on purpose from $Li_2(pyrmP^tBu_2)_2CMe_2$ and $GeCl_4$. Therefore, the reaction of **E** with $CuCl_2$ involves an unexpected redox process where the Ge^{II} atom of **E** is oxidized to Ge^{IV} (in **5**) by the Cu^{II} atom of $CuCl_2$, which is reduced to Cu^{I} (in **4**).

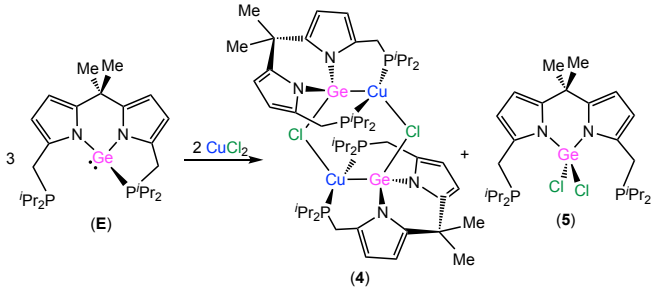

Scheme 3. Reaction of germylene **E** with $CuCl_2$.

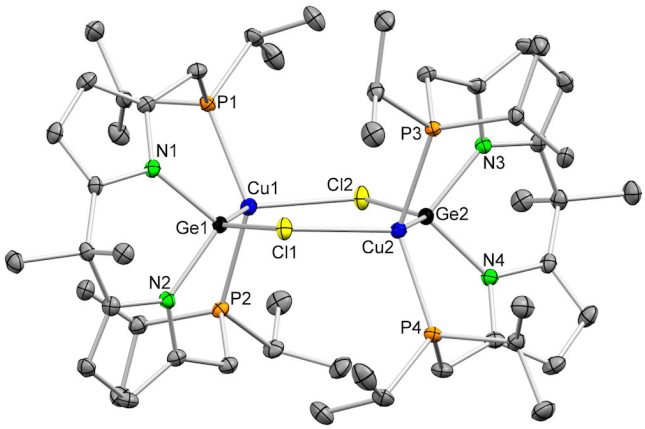

Figure 9. XRD molecular structure of complex **4** (30% displacement ellipsoids, H atoms have been omitted for clarity). Selected bond lengths (Å) and angles (°): Cu1−P1 2.2781(8), Cu1−P2 2.2890(8), Cu1−Ge1 2.3785(5), Cu1−Cl2 2.4048(8), Ge1−Cl1 2.3635(7); Cl1−Ge1−Cu1 131.20(2), Ge1−Cu1−Cl2 118.38(2), P1−Cu1−P2 138.53(3).

The NMR spectra of complex **4** were very similar to those of complex **3**, also suggesting average C_S symmetry, but its dimeric nature was confirmed by XRD (Figure 9). The molecule is formed by two [Cu{μ-κ^3*P*,*Ge*,*P*-GeCl(pyrmP^{t}Bu$_2$)$_2$CMe$_2$}] units connected to each other in such a way that the Cl atom of one unit is attached to the Cu atom of the other unit, thus forming an almost planar but irregular six-membered $Cl_2Cu_2Ge_2$ ring. In this case, both the Ge and Cu atoms are in approximate tetrahedral environments, with a Ge–Cu bond distance of 2.3785(5) Å. A related mononuclear copper(I) complex, [Cu{μ-κ^3*P*,*Ge*,*P*-GeCl(pyrmP^{t}Bu$_2$)$_2$CMe$_2$}(PPh$_3$)], in which the Cu atom also shows a tetrahedral coordination, has been previously prepared by treating germylene **E** with the copper(I) complex [Cu$_4$(μ$_3$-Cl)$_4$(PPh$_3$)$_4$] in 1 to 1/4 mole ratio.[13] Di- and tetranuclear copper(I) complexes, with structures quite different from that of **4**, have been reported to result from reactions of germylene **B** (Figure 1) with CuCl.[11]

Germylene **E** also reacted with $ZnCl_2$ at room temperature. The only product of this reaction was the mononuclear complex [ZnCl{μ-κ^3*P*,*Ge*,*P*-GeCl(pyrmP^{t}Bu$_2$)$_2$CMe$_2$}] (**6**) (Scheme 6), which also presents a symmetry plane in solution (NMR).

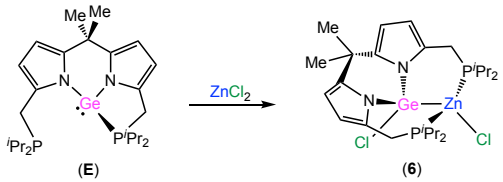

Scheme 4. Synthesis of complex **6**.

The molecular structure of complex **6** was determined by XRD (Figure 10). In this case, as commonly found for four-coordinate zinc(II) complexes, the Zn atom is in a tetrahedral environment, the Ge–Zn bond distance being 2.4705(3) Å. Complex **6** is the first PGeP pincer zinc complex to be reported.

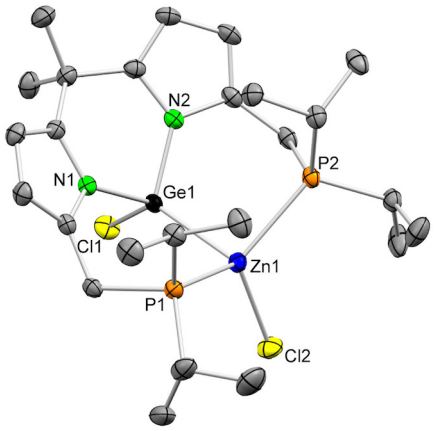

Figure 10. XRD molecular structure of complex **6** (30% displacement ellipsoids, H atoms have been omitted for clarity). Selected bond lengths (Å) and angles (°): Zn1−P1 2.4112(6), Zn1−P2 2.4440(6), Zn1−Ge1 2.4705(3), Zn1−Cl2 2.2314(6), Ge1−Cl1 2.2265(5), Cl1−Ge1−Zn1 126.31(2), Ge1−Zn1−Cl2 116.78(2), P1−Zn1−P2 129.16(2).

Conclusions

The reactions of germylene **E** with a series of first-raw transition metal (Fe–Zn) dichlorides afforded in all cases reaction products that contain a PGeP chloridogermyl ligand that arises from the insertion of the divalent Ge atom of germylene **E** into an M–Cl bond.

While the iron(II) complex **1** is square planar with intermediate spin state (S^1) over the temperature range 50–380 K, the cobalt(II) complex **2** presents an unusual gradual spin crossover behavior, involving two square planar species with spin states $S^{1/2}$ and $S^{3/2}$, which shows a linear dependence between μ_{eff} and T that extends over several hundred degrees (10–380 K).

Complex **4**, which resulted from a redox process between germylene **E** (reductant) and $CuCl_2$ (oxidant), is a binuclear species containing an almost planar inorganic six-membered $Cl_2Cu_2Ge_2$ ring.

The reactions described in this manuscript demonstrate that germylene **E** is an excellent precursor to complexes containing a κ^3-PGeP cloridogermyl ligand that is able to hold the metal atoms not only in a planar pocket, as occurs in the square planar complexes **1**–**3**, but also in a tripodal pocket, as occurs in complexes **4** and **6**, which have their metal atoms in tetrahedral ligand environments.

No doubt, the results reported herein will prompt the synthesis of many more PGeP pincer transition metal derivatives with interesting structural, magnetic, bonding and/or catalytic properties.[33]

Experimental

Detailed synthetic procedures and analytical, spectroscopic, structural (XRD) and computational (DFT) data for compounds **1**–**6** are given in the Supporting Information. CCDC deposition numbers: 2047806 ($\mathbf{2}_{157K}$), 2057042 ($\mathbf{2}_{298K}$), 2047807 (**3**), 2047808 (**4**) and 2047809 (**6**).

Acknowledgements

This work has been supported by research grants obtained from *Ministerio de Economía y Competitividad* (CTQ2016-75218-P, CTQ2016-78205-P and RED2018-102387-T) and *Agencia Estatal de Investigación* (PID2019-104652GB-100 and PID2019-106184GB-100). The authors would like to acknowledge the technical support provided by *Servicios Científico-Técnicos de la Universidad de Oviedo* and *Servicio General de Apoyo a la Investigación-SAI de la Universidad de Zaragoza*. Daniel Joven is thanked for his kind assistance in the preparation of the EPR samples.

Conflicts of interest

The authors declare no conflict of interest.

Keywords: PGeP pincers · germylenes · pincer complexes · first-row metals · spin crossover

References

[1] For selected recent reviews on pincer complexes and their applications, see: a) E. Peris, R. H. Crabtree, *Chem. Soc. Rev.* 2018, **47**, 1959–1968; b) *The Privileged Pincer–Metal Platform: Coordination Chemistry & Applications*, ed. G. van Koten, R. A. Gossage, Springer, Cham, **2016**; c) M. Asay and D. Morales-Morales, *Dalton Trans.* **2015**, *44*, 17432–17447; d) C. Gunanathan and D. Milstein, *Chem. Rev.*, **2014**, *114*, 12024–12087; e) *Organometallic Pincer Chemistry*, ed. G. van Koten, D. Milstein, Springer, Heidelberg, **2013**; f) S. Schneider, J. Meiners, B. Askevold, *Eur. J. Inorg. Chem.* **2012**, 412–429.

[2] For selected reviews on pincer complexes in homogeneous catalysis, see: a) G. Bauer, X. Hu, *Inorg. Chem. Front,* **2016**, *3*, 741–765; b) H. A. Yonus, W. Su, N. Ahmad, S. Chen, F. Verpoort, *Adv. Synth. Catal.* **2015**, *357*, 283–330; c) *Pincer and Pincer-Type Complexes: Applications in Organic Synthesis and Catalysis*, ed. K. J. Szabó, O. F. Wendt, Wiley-VCH, Weinheim, **2014**; d) Q.-H. Dend, R. L. Melen, L. H. Gade, *Acc. Chem. Res.* **2014**, *47*, 3162–3173.

[3] See, for example: a) X. Ren, M. Wesolek, P. Braunstein, *Chem. Eur. J.* **2018**, *24*, 14794–14801; b) A. Eizawa, S. Nishimura, K. Arashiba, K. Nakajima, Y. Nishibayashi, *Organometallics* **2018**, *37*, 3086–3892; c) A. Eizawa, K. Arashiba, H. Tanaka, S. Kuriyama, Y. Matsuo, K. Nakajima, K. Yoshizawa, Y. Nishibayashi, *Nat. Commun.* **2017**, *8*, 14874/1–14874/12; d) A. G. Nair, R. T. McBurney, M. R. D. Gatus, D. B. Walker, M. Bhadbhade, B. A. Messerle, *J. Organomet. Chem.* **2017**, *845*, 63–70; e) D. A. Valyaev, J. Willot, L. P. Mangin, D. Zargarian, N. Lugan, *Dalton Trans.* **2017**, *46*, 10193–10196; f) K. Farrel, M. Albrecht**,** in *The Privileged Pincer–Metal Platform:*

Coordination Chemistry & Applications, ed. G. van Koten, R. A. Gossage, Springer, Cham, **2016**, p. 45.

[4] a) Z. Benedek, T. Szilvási, *Organometallics* **2017**, *36*, 1591–1600; b) A. Rosas-Sánchez, I. Alvarado-Beltrán, A. Baceiredo, N. Saffon-Merceron, S. Massou, V. Ranchadell, T. Kato, *Angew. Chem. Int. Ed.* **2017**, *56*, 10549–10554; c) Y.-P. Zhou, S. Raoufmoghaddam, T. Szilvási, M. Driess, *Angew. Chem. Int. Ed,* **2016**, *55*, 12868–12884; d) T. Troadec, A. Prades, R. Rodriguez, R. Mirgalet, A. Baceiredo, N. Saffon-Merceron, V. Branchadell, T. Kato, *Inorg. Chem.* **2016**, *55*, 8234–8240; e) J. A. Cabeza, P. García-Álvarez, R. Gobetto, L. González-Álvarez, C. Nervi, E. Pérez-Carreño, D. Polo, *Organometallics* **2016**, *35*, 1761–1770; f) Z. Benedek, T. Szilvási, *RSC Adv.* **2015**, *5*, 5077–5086; g) L. Álvarez-Rodríguez, J. A. Cabeza, P. García-Álvarez, D. Polo, *Coord. Chem. Rev.* **2015**, *300*, 1–28; h) G. Tan, S. Enthaler, S. Inoue, B. Blom, M. Driess, *Angew. Chem. Int. Ed.* **2015**, *54*, 2214–2218; i) L. Álvarez-Rodríguez, J. A. Cabeza, P. García-Álvarez, E. Pérez-Carreño, D. Polo, *Inorg. Chem.* **2015**, *54*, 2983–2994; j) J. A. Cabeza, P. García-Álvarez, E. Pérez-Carreño, D. Polo, *Chem. Eur. J.* **2014**, *20*, 8654–8663.

[5] For a recent review on silylene transition-metal complexes in catalysis, see: Y.-P. Zhou, M. Driess, *Angew. Chem. Int. Ed.* **2019**, *58*, 3715–3728.

[6] See, for example: a) Y.-P. Zhou, Z. Mo, M.-P. Luecke, M. Driess, *Chem. Eur. J.* **2018**, *24*, 4780–4784; b) J. A. Cabeza, P. García-Álvarez, L. González-Álvarez, *Chem. Commun.* **2017**, *53*, 10275–10278; c) T. Iimura, N. Akasaka, T. Kosai, T. Iwamoto, *Dalton Trans.* **2017**, *46*, 8868–8874; d) H. Ren, Y.-P. Zhou, Y. Bai, C. Cui, M. Driess, *Chem. Eur. J.* **2017**, *23*, 5663–5667; e) T. Iimura, N. Akasaka, T. Iwamoto, *Organometallics* **2016**, *35*, 4071–4076; f) L. Álvarez-Rodríguez, J. A. Cabeza, J. M Fernández-Colinas, P. García-Álvarez, D. Polo, *Organometallics* **2016**, *35*, 2516–2523; g) Y.-P. Zhou, S. Raoufmoghaddam, T. Szilvási, M. Driess, *Angew. Chem. Int. Ed.* **2016**, *55*, 12868–12872; h) T. T. Metsänen, D. Gallego, T. Szilvási, M. Driess, M. Oestreich, *Chem. Sci.* **2015**, *6*, 7143–7149; i) D. Gallego, S. Inoue, B. Blom, M. Driess, *Organometallics* **2014**, *33*, 6885–6897; j) D. Gallego, A. Brück, E. Irran, F. Meier, F. Kaupp, M. Driess, *J. Am. Chem. Soc.* **2013**, *135*, 15617–15626; k) A. Brück, D. Gallego, W. Wang, E. Irran, M. Driess, J. F. Hartwig, *Angew. Chem. Int. Ed.* **2012**, *51*, 11478–11482; l) S. Li, Y. Wang, W. Yang, K. Li, H. Sun, X. Li, O. Fuhr, D. Fenske, *Organometallics* **2020**, *39*, 757–766; m) N. Parvin, B. Mishra, M. Neralkar, J. Hossain, P. Parameswaran, S. Hotha, S. Kahn, *Chem. Commun.* **2020**, *56*, 7625–7628; n) R. Arevalo, T. P. Pabst, P. J. Chirik, *Organometallics* **2020**, *39*, 2763.

[7] W. Wang, S. Inoue, E. Irran, M. Driess, *Angew. Chem. Int. Ed.* **2012**, *51*, 3691–3694.

[8] a) M. T. Whited, J. Zhang, S. Ma, B.D. Nguyen, D. E. Janzen, *Dalton Trans.* **2017**, *46*, 14757–14761; b) J. C. DeMott, W. X. Gu, B. J. McCulloch, D. E. Herbert, M. D. Goshert, J. R. Walensky, J. Zhou, O. V. Ozerov, *Organometallics* **2015**, *34*, 3930–3933; c) H. Handwerker, M. Paul, J. Blumel, C. Zybill, *Angew. Chem. Int. Ed.* **1993**, *32*, 1313–1315.

[9] a) Y. Cabon, H. Kleijn, M. A. Siegler, A. L. Spek, R. J. M. Gebbink, B.-J. Deelman, *Dalton Trans*. **2010**, *39*, 2423–2427; b) S. Warsink, E. J. Derrah, C. A. Boon, Y. Cabon, J. J. M. de Pater, M. Lutz, R. J. M. Gebbink, B.-J. Deelman, *Chem. Eur. J*. **2015**, *21*, 1765–1779.

[10] L. Álvarez-Rodríguez, J. Brugos, J. A. Cabeza, P. García-Álvarez, E. Pérez-Carreño, D. Polo, *Chem. Commun.* **2017**, *53*, 893–896.

[11] S. Bestgen, N. H. Rees, J. M. Goicoechea, *Organometallics* **2018**, *37*, 4147–4155.

[12] J. A. Cabeza, I. Fernández, J. M. Fernández-Colinas, P. García-Álvarez and C. J. Laglera-Gándara, *Chem. Eur. J.* **2019**, *25*, 12423-12430.

[13] J.A. Cabeza, I. Fernández, P. García-Álvarez, C. J. Laglera-Gándara, *Dalton Trans.* **2019**, *48*, 13273–13280.

[14] T. Watanabe, Y. Kasai, H. Tobita, *Chem. Eur. J.* **2019**, *25*, 13491-13495.

[15] J. A. Cabeza, P. García-Álvarez, C. J. Laglera-Gándara, *Eur. J. Inorg. Chem.* **2020**, 748-795.

[16] a) J. Brugos, J. A. Cabeza, P. García-Álvarez, E. Pérez-Carreño, D. Polo, *Dalton Trans.* **2018**, *47*, 4534–4544; b) L. Álvarez-Rodríguez, J. Brugos, J. A. Cabeza, P. García-Álvarez, E. Pérez-Carreño, *Chem. Eur. J.* **2017**, *23*, 15107–15115; c) J. Brugos, J. A. Cabeza, P. García-Álvarez, E. Pérez-Carreño, *Organometallics* **2018**, *37*, 1507–1514.

[17] J. A. Cabeza, P. García-Álvarez, C. J. Laglera-Gándara, E. Pérez-Carreño, *Chem. Commun*. **2020**, *56*, 14095–14097.

[18] S. Bestgen, M. Mehta, T. C. Johnstone, P. W. Roesky, J. M. Goicoechea, *Chem. Eur. J.* **2020**, *26*, 9024–9031.

[19] R. Boca, *Coord. Chem. Rev*. **2004**, *248*, 757–815.

[20] a) C. Hu, B. C. Noll, C. E. Schulz, W. E. Acheidt, *Inorg. Chem.* **2007**, *46*, 619–621; b) K. Ray, A. Begum, T. Weyhermüller, S. Piligkos, J. van Slageren, F. Neese, K. Wieghart, *J. Am. Chem. Soc*. **2005**, *127*, 4403–4415.

[21] See, for example: a) C. V. Thomson, H. D. Arman, Z. J. Tonzetich, *Organometallics* **2019**, *38*, 2979–2989; b) Z. Ouyang, L. Deng, *Organometallics* **2013**, *32*, 7268–7271.

[22] W. R. Scheidt, C. A. Reed, *Chem. Rev.* **1981**, *81*, 543–555.

[23] See, for example: a) M. E. Pascualini, N.V. Di Russo, A. E. Thuijs, A. Ozaroeski, S. A. Stoian, K. A. Abboud, G. Chistou, A. S. Veige, *Chem. Sci.* **2015**, *6*, 608–612; b) S. A. Cantalupo, S. R. Fiedler, M. P. Shores, A. L. Rheingold, L. H. Doerrer, *Angew. Chem. Int. Ed.* **2012**, *51*, 1000–1005.

[24] For general information on spin crossover, see, for example: a) D. J. Harding, P. Harding, W. Phonsri, *Coord. Chem. Rev.* **2016**, *313*, 38–61; b) I. Krivokapic, M. Zeara, M. L. Daku, A. Vargas, C. Enachescu, C. Ambrus, P. Tregenna-Piggott, N. Amstutz, A. Hauser, *Coord. Chem. Rev.* **2007**, *251*, 364–378; c) P. Gütlich, A. B. Gaspar, Y. García, *Beilstein J. Org. Chem*. **2013**, *9*, 342–391.

[25] For examples of gradual spin crossover: see, for example: a) Y. Horii, Y. Kanegae, K. Takahashi, A. Fuyuhiro, M. Noguchi, H. Suzuki, M. Nakano*, Inorg. Chem.* **2020**, *59*, 5418–5423; b) R. Kulmaczewski, O. Cespedes, M. A. Halcrow, *Inorg. Chem.* **2017**, *56*, 3144–3148; c) A. L. Nivorozhkin, H. Toftlund, M. Nielsen, *J. Chem. Soc., Dalton Trans.* **1994**, 361–367.

[26] See, for example: a) H. E. Mason, W. Li, M. A. Carpenter, M. L. Hamilton, J. A. K. Howard, H. A. Sparkes, *New. J. Chem.* **2016**,*40*, 2466-2478; b) P. Guionneau, F. Le Gac, S. Lakhoufi, A. Kaiba, J.-F. Létard, P. Négrier, D. Mondieig, J. A. K. Howard, J.-M. Léger, *J. Phys. Cond. Mat.* **2007**, *19*, 326211–326222.

[27] a) J. Cirera, P. Alemany, S. Alvárez, *Chem. Eur. J.* **2004**, *10*, 190–207; b) J. Cirera, E. Ruiz, S. Alvárez, *Inorg. Chem.* **2008**, *47*, 2871–2889.

[28] M. E. Pascualini, S. A. Stoian, A. Ozarowski, N. V. Di Russo, A. E. Thuijs, K. A. Abboud, G. Christou, A. S. Veige, *Dalton Trans.* **2015**, *44*, 20207–20215.

[29] E. M. Schubert, *J. Chem. Educ.* **1992**, *69*, 62.

[30] H. Drulis, K. Dyrek, K. P. Hoffmann, S. K. Hoffmann, A. Weselucha-Birczynska, *Inorg. Chem.* **1984**, *24*, 4009-4012.

[31] D. Attanasio, *Chem. Phys. Lett*, **1977**, *49*, 547-549.

[32] B. R. McGarvey, *Can. J. Chem.* **1975**, *53*, 2498–2511.

[33] Some PGeP germyl metal complexes have already demonstrated an interesting catalytic activity: a) C. Zhu, J. Takaya, N. Iwasawa, *Org. Lett.* **2015**, *17***,** 1814; b) f) J. Takaya, S. Nakamura, N. Iwasawa, *Chem. Lett.* **2012** *,41***,** 967–975.

Entry for the Table of Contents

PGeP pincers

FULL PAPER

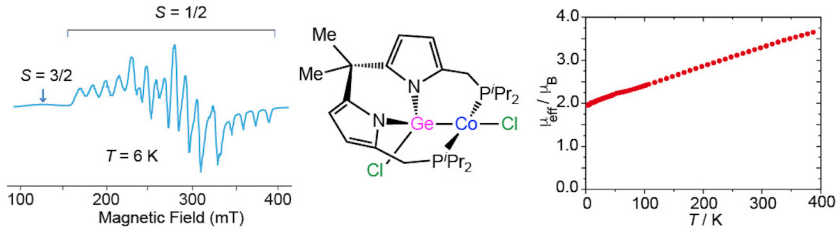

A. Arauzo, J. A. Cabeza, I. Fernández, P. García-Álvarez, I. García-Rubio and C. J. Laglera-Gándara*

Page No. – Page No.

Reactions of Late First-Row Transition Metal (Fe–Zn) Dichlorides with a PGeP Pincer Germylene

Paramagnetic (M = Fe^{II}, Co^{II}) and diamagnetic (M = Ni^{II}, Cu^{I}, Zn^{II}) mononuclear (M = Fe^{II}, Co^{II}, Ni^{II}, Zn^{II}) and binuclear (M = Cu^{I}) complexes supported by a PGeP pincer chloridogermyl ligand have been prepared from reactions of a dipyrromethane-derived PGeP germylene with the corresponding metal(II) chlorides.

ORCID Identifiers

Ana Arauzo	http://orcid.org/0000-0002-5999-341X
Javier A. Cabeza	http://orcid.org/0000-0001-8563-9193
Israel Fernández	http://orcid.org/0000-0002-0186-9774
Pablo García-Álvarez	http://orcid.org/0000-0002-5024-3874
Inés García-Rubio	http://orcid.org/0000-0002-1827-1250
Carlos J. Laglera-Gándara	http://orcid.org/0000-0002-4480-1315